Pergamon

Progress in Surface Science, Vol. 48, Nos. 1–4, pp. 27–38, 1995
Copyright © 1995 Elsevier Science Ltd
Printed in the USA. All rights reserved
0079-6816/95 $29.00 + .00

0079-6816(95)E00006-2

ADSORPTION OF NOBLE GASES ON METAL SURFACES AND THE SCANNING TUNNELING MICROSCOPE

F. Flores, P.L. de Andres †, F.J. Garcia-Vidal,

L. Jurczyszyn*, N. Mingo, and R. Perez

Departamento de Fisica de la Materia Condensada, C-XII,

Facultad de Ciencias, Universidad Autonoma de Madrid, E-28049 Madrid (SPAIN),

and

† *Instituto de Ciencia de Materiales (CSIC), C-XII,*

Facultad de Ciencias, Universidad Autonoma de Madrid, E-28049 Madrid (SPAIN)

Abstract

Physisorption on metal surfaces, and the tunneling currents through the adsorbed species, are calculated using a unified formalism that presents both problems on the same footing. Our method is based on a self-consistent LCAO approach whereby the different interaction parameters defining the bonds, and the tunneling currents, are calculated using the atomic properties of the atomic species forming the interface. Green function methods and the Keldish formalism are used to calculate the different physical properties. We present results for xenon adsorbed on aluminum.

Abbreviations

STM Scanning Tunneling Microscope
LCAO Linear Combination of Atomic Orbitals

1. Introduction

Recent research in the field of the STM has shown how to control the position of atoms on different surfaces, move them along the surface and even transfer them between the tip and the sample by applying a suitable voltage [1-4].

The first results in this field were obtained with xenon adsorbed on a nickel surface [5], and although the main mechanism explaining the atomic transport process has been described using a semi-empirical approach [6], we still lack a more fundamental approach that yields on the same footing both, the xenon-metal interaction including the effects due to the metal lattice, and the tunneling currents across the adsorbate.

The aim of this paper is to present a unified treatment of both, the interaction of rare gas atoms with metal surfaces, and the tunneling currents across the microscope interface. In section 2 we discuss our formalism, while in section 3 we present our results for xenon adsorbed on aluminum. We should stress that the general formulation discussed in section 2 is the combination of the different approaches presented in previous works [7-10].

2. Formalism: Interaction Potential and the Tunneling Currents

In Fig.1 we show the geometry we are interested in: a rare gas atom (a) is adsorbed on a metal and we start to explore this surface geometry by calculating the tunneling currents between the tip (T) and the surface (S). In our formalism we use a LCAO approach to describe the tip-atom-sample interaction by means of the general Hamiltonian:

$$\hat{H} = \hat{H}_T + \hat{H}_S + \hat{H}_a + \hat{H}_{int} \tag{1}$$

where $\hat{H}_T$ and $\hat{H}_S$ are the tip and sample Hamiltonians, H_a the rare gas atom Hamiltonian, $\sum_\alpha E_\alpha c^\dagger_{\alpha,\sigma} c_{\alpha,\sigma}$, and

$$\hat{H}_{int} = \sum_{\alpha,i} T^L_{\alpha,i}(c^\dagger_{i,\sigma} c_{\alpha,\sigma} + c^\dagger_{\alpha,\sigma} c_{i,\sigma}) + \sum_{\alpha,j} T^R_{\alpha,j}(c^\dagger_{j,\sigma} c_{\alpha,\sigma} + c^\dagger_{\alpha,\sigma} c_{j,\sigma}) + \sum_{i,j} T^{LR}_{i,j}(c^\dagger_{i,\sigma} c_{j,\sigma} + c^\dagger_{j,\sigma} c_{i,\sigma}) \tag{2}$$

defines the interaction between the rare-gas levels, α, and the different orbitals on the tip (L) and the sample (R), and the interaction between the tip and the sample.

Tunneling currents between the rare gas atom-sample composite, A, and the tip can be calculated if the coefficients $T^L_{\alpha,i}$, and $T^{LR}_{i,j}$ (T_{LA} hereafter), are known. Using the Keldish's

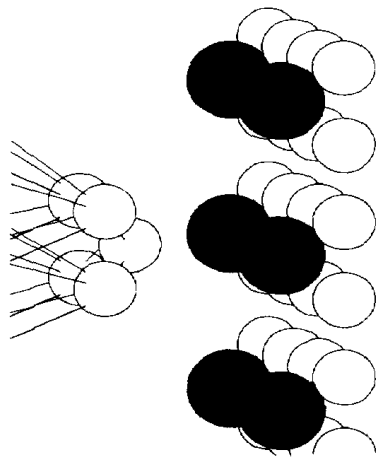

FIG. 1. Geometry for the interface tip/adsorbed-atom/sample. Shaded circles represent xenon atoms.

Green function method, as applied by Caroli et al. [11,12], the tunneling current, J, between the tip and the rare gas atom-sample composite is given by:

$$J = -i\frac{2e}{\hbar}\sum_{L,A} T_{L,A}(< c_L^\dagger c_A > - < c_A^\dagger c_L >) \tag{3}$$

where <> is the mean expectation value in the stationary state defined by the applied bias. Equation (3) can be written as a function of the Keldish's Green functions components, $G_{LA}^{+,-}$ [11], as follows:

$$J = \frac{e}{\pi\hbar}\sum_{L,A} T_{LA}\int_{-\infty}^{\infty} d\omega[G_{LA}^{+,-}(\omega) - G_{AL}^{+,-}(\omega)] \tag{4}$$

These Green functions components can be calculated by solving a Dyson-like equation, relating the Green functions of the total system to the Green functions of each independent surface coupled by the hopping terms, T_{LA}. In this approach the xenon-sample system forms a simple entity. Details can be found elsewhere [12], let us only mention here that the total current, J, can be written as follows:

$$J = \frac{4\pi e}{\hbar}\int_{-\infty}^{\infty} d\omega Tr[\hat{T}_{LA}\rho_{AA}^0(\omega)D_{AA}^r(\omega)\hat{T}_{AL}^\dagger\rho_{LL}^0(\omega)D_{LL}^a(\omega)][f_L(\omega) - f_A(\omega)] \tag{5}$$

where,

$$D_{LL}^a(\omega) = [\hat{I} - \hat{T}_{LA}G_{AA}^{a(0)}\hat{T}_{AL}^\dagger G_{LL}^{a(0)}]^{-1} \tag{6}$$

and,

$$D_{AA}^r(\omega) = [\hat{I} - \hat{T}_{AL}G_{LL}^{r(0)}\hat{T}_{LA}^\dagger G_{AA}^{r(0)}]^{-1} \tag{7}$$

$G^{a(0)}$ and $G^{r(0)}$ being the advanced and retarded Green functions of the uncoupled system (with $T_{LA} = 0$); ρ^0 refers to the density of states ($\rho^0 = -\frac{1}{\pi}ImG^{r(0)}$), and $f_{L,A}$ are the Fermi distribution functions for the tip and the adsorbate-sample composite, respectively.

Equation (5) yields the tunneling current if the different hopping terms, $\hat{T}_{LA}$, are known. We shall turn our attention now to discussing how the different T_{LA} can be calculated. To this end, we start by considering the one-electron Hamiltonian, $\hat{H}$, associated with all the atoms forming the interface (the tip, the sample, and the adsorbate). Eigenfunctions of $\hat{H}$ can be obtained using a LCAO method:

$$\Psi = \sum_{i,n} C_{i,n}\psi_{i,n}$$

i referring to a particular atom and n to a particular orbital. Then, eigenstates of $\hat{H}$ are given by the secular equation:

$$det| < \psi_{i,n}|\hat{H} - E|\psi_{j,n'} > | = 0 \tag{8}$$

It is convenient to introduce the Löwdin's basis:

$$\Phi_a = \sum_{a'}(S^{-1/2})_{a,a'}\psi_{a'}$$

where, $S_{a,a'} =< \psi_a|\psi_{a'} >$ $(a \equiv (i,n))$, and to write the matrix defining the secular equation as follows:

$$-E\hat{I}_{a,a'} + (S^{-1/2})_{a,b}H_{b,b'}(S^{-1/2})_{b',a'} \tag{9}$$

where $\hat{I}_{a,a'}$ is the unit matrix. This last equation, defines the effective Hamiltonian,

$$\hat{H}_{eff} = S^{-1/2}\hat{H}S^{-1/2} \tag{10}$$

for our initial system.

Rare gas atoms have a small overlap with other atoms and, it is natural to calculate $\hat{H}_{eff}$ which, by expanding $S^{-1/2}$ up to second order in the overlap coefficients, $S_{a,a'}$, yields:

$$(H_{eff})_{a,a} = H_{a,a} + \frac{1}{4}\sum_b S^2_{a,b}(H_{a,a} - H_{b,b}) - \sum_{a\neq b} S_{a,b}T_{b,a} \tag{11a}$$

$$(H_{eff})_{a,b} = T_{a,b} = H_{a,b} - \frac{1}{2}S_{a,b}(H_{a,a} + H_{b,b}) \tag{11b}$$

Equations (11) show how a rare gas atom interact with the tip or the sample. In particular, (11b) yields the hopping interaction between orbitals a and b; it can be shown [7] that $T_{a,b}$ can be well approximated by:

$$T_{a,b} = -\frac{\gamma}{2}\int dS(\psi_a\nabla\psi_b - \psi_b\nabla\psi_a) \tag{12}$$

where γ is a coefficient that typically takes values in the range of 1.3 to 1.5. Equation (12) relates the hopping parameters, $T_{a,b}$, to the Bardeen tunneling current, $T^B_{a,b}$, associated with the wavefunctions, ψ_a and ψ_b.

Equation (11b) establishes the link between the tunneling currents and the hopping integrals appearing between the rare gas and the tip or the sample. It is now important

to realize that the terms $\frac{1}{4}\sum_b S^2_{a,b}(H_{a,a} - H_{b,b})$ and $-\sum_{a\neq b} S_{a,b}T_{a,b}$ represent the repulsive interaction appearing between the electronic clouds of different atoms that tend to increase the kinetic energy of the system when overlapping.

Then, the one-electron part of Hamiltonian (1) describing the interaction of the rare gas with the interface, can be written as follows:

$$\hat{H}^{inter} = \sum_{i,\sigma} E_i \hat{n}_{i,\sigma} + \sum_{j,\sigma} E_j \hat{n}_{j,\sigma} + \sum_{\alpha,\sigma} E_\alpha \hat{n}_{\alpha,\sigma} + \sum_{i,\alpha,\sigma} T_{i,\alpha}(c^\dagger_{i,\sigma}c_{\alpha,\sigma} + c^\dagger_{\alpha,\sigma}c_{i,\sigma}) + \\ + \sum_{j,\alpha,\sigma} T_{j,\alpha}(c^\dagger_{j,\sigma}c_{\alpha,\sigma} + c^\dagger_{\alpha,\sigma}c_{j,\sigma}) \tag{13}$$

where E and T are given by (11a) and (11b), respectively.

It is interesting to stress that the terms $[\frac{1}{2}S^2_{a,b}(H_{a,a} - H_{b,b}) - S_{a,b}T_{a,b}]$ play a crucial role in describing the repulsion between rare gases and metal orbitals. This can be understood by considering the interaction of a fully occupied rare gas orbital, E_1, and a partially occupied level of the metal, E_2. One can prove that, for this case, $T_{1,2}$ can be approximated by [8] $-\frac{1}{2}S_{1,2}(E_2 - E_1)$. Then, considering only the one electron terms, one reaches the conclusion that the levels, E_1 and E_2, are shifted by the following quantities:

$$\delta E_1 = 0; \quad \delta E_2 = S^2_{1,2}(E_2 - E_1)$$

This metal level shift measures the contribution of the one electron terms to the repulsive potential between the occupied rare gas orbitals and the metal.

The total rare gas-metal interaction is obtained by adding the Coulomb interaction term to Hamiltonian (13):

$$\hat{H}^{Coulomb} = \frac{1}{2}\sum_{i,\alpha,\sigma}(J_{i,\alpha}\hat{n}_{i,\sigma}\hat{n}_{\alpha,\sigma} + \tilde{J}_{i,\alpha}\hat{n}_{i,\sigma}\hat{n}_{\alpha,\sigma}) + \frac{1}{2}\sum_{j,\alpha,\sigma}(J_{j,\alpha}\hat{n}_{j,\sigma}\hat{n}_{\alpha,\sigma} + \tilde{J}_{j,\alpha}\hat{n}_{j,\sigma}\hat{n}_{\alpha,\sigma}) \tag{14}$$

here, $J_{i,\alpha}$ measures the Coulomb interaction between orbitals i and α, while $\tilde{J}_{i,\alpha} = J_{i,\alpha} - J_{x,i\alpha} + J_{i,j}S^2_{i,j}$, $J_{x,i\alpha}$ being the exchange interaction between the same orbitals i and α.

The contributions arising from Hamiltonian (14) can be analyzed using an approximation that yields the exchange-correlation energy associated with the interaction between an orbital α and the metal orbitals j. Following reference [13], we can write for the exchange-correlation energy associated with the orbital α, σ:

$$E^{xc}_{\alpha,\sigma} = -\frac{1}{2}\overline{J_\alpha} n_{\alpha,\sigma} \times (1 - n_{\alpha,\sigma}) \tag{15}$$

where $n_{\alpha,\sigma}$ is the mean occupation number of the α, σ-orbital, and $\overline{J_\alpha}$ an average interaction between the $n_{\alpha,\sigma}$-charge and its exchange-correlation hole $(1 - n_{\alpha,\sigma})$.

Following Kohn and Sham [14], we introduce the following local potential, V^{xc}, associated with the exchange-correlation energy:

$$V^{xc}_{\alpha,\sigma} = \frac{\partial E^{xc}}{\partial n_{\alpha,\sigma}} = -\overline{J_\alpha} \times (\frac{1}{2} - n_{\alpha,\sigma}) \tag{16}$$

In particular, for the almost empty xenon 6s level, $n_{\alpha,\sigma} \approx 0$, and $V^{xc}_{\alpha,\sigma}$ describes the image potential that lowers that level towards the metal Fermi energy.

Equations (15) and (16) have been used to calculate the many-body effects between the rare gas atom levels and the surface. In particular, for xenon, this analysis has been applied to the 6s and 5p orbitals that change their occupations slightly with respect to the free-atom occupancies. Other filled orbitals have full occupancies, and their exchange-correlation interaction is negligible accordingly.

In summary, the short-range interaction of the rare gas with the metal surface is calculated in the following way:

(i) The repulsive interaction associated with the overlap between different orbitals is calculated using equation (11a).

(ii) The hopping integrals, $T_{i,\alpha}$ or $T_{j,\alpha}$, define a hybridization energy between the rare gas atom and the surface that is interpreted in terms of a binding energy.

(iii) The exchange-correlation contribution given by (15) and (16) has to be added to the previous terms

(iv) Finally, an electrostatic term is also calculated. This term takes into account the Coulomb interaction associated with the small charge transfer that can appear between the adsorbed atom and the surface.

Therefore, the total (short-range) interaction between the rare gas and the surface appears as the sum of four different contributions: repulsive overlap interaction, hybridization, exchange-correlation and electrostatic energies. Results for the interaction of xenon with aluminum will be displayed showing those different contributions.

3. Results

3.1. Adsorption of xenon on aluminum

In our calculation of the adsorption of xenon on aluminum, we describe the metal surface using conventional tight-binding parameters [19]. Thus, the method presented above has been applied to the calculation of the xenon-metal interaction. To this end, atomic wavefunctions and the xenon energy levels have been taken from atomic tables or standard atomic calculations [15].

The total xenon-metal potential is obtained by adding to the short range potential the van der Waals interaction:

$$V_{vdW} \approx \frac{c_3}{(z - z_{vdW})^3} \tag{17}$$

where z_{vdW} is the reference plane. Saturation effects, for $z \to z_{zdW}$, are taken into account as discussed by Tang and Toennies [16]. We have used in (17) the conventional parameters given in the literature [17,18].

Figure 2a shows the xenon-aluminum interaction for xenon approaching the metal surface along the top and center positions on Al(100). The minimum in the interaction energy appears for the center position, around a xenon-aluminum distance of $d \approx 4.6$ Å; this position is more favourable than the top one, due basically to larger hopping integrals

between xenon and the metal that increase the hybridization and the many-body energies. This point is better understood if we split the short-range xenon-aluminum interaction into its different contributions: repulsive, electrostatic, hybridization and many-body energies. Figure 2b shows those contributions for xenon located on the top position (similar results are found for the center position [20]).

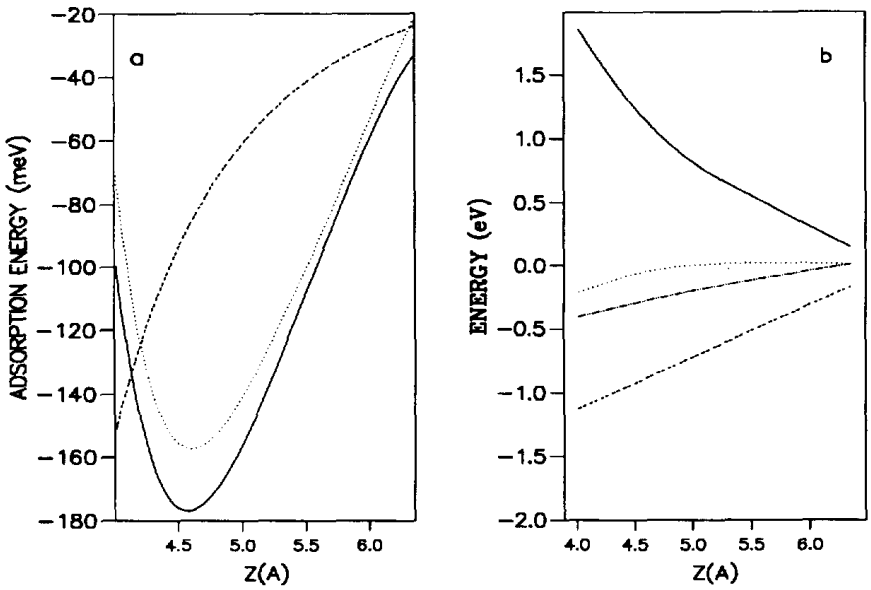

FIG. 2. (a) Xe/Al(100) total interaction for hollow (full line), top (dotted line) adsorption sites, and long-range van der Waals contribution (broken line). (b) Different short-ange contributions are shown for top site (full: kinetic repulsion, broken: hybridization, dotted: electrostatic, broken-dotted: exchange and correlation).

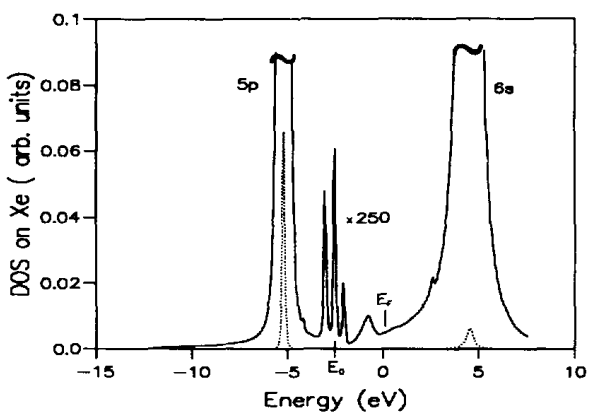

FIG. 3 Density of states on the xenon atom for the center equilibrium position of Fig. 2a. E_0 is the charge neutrality level.

For rare gas atoms of small size (e.g. helium), the typical atom-surface interaction shows a repulsive term that controls the short-range interaction potential for all distances; for xenon things are different due to the role played mainly by the 6s orbitals. The point to realize is the following: due to the interaction of those orbitals with the metal, we find that some charge is transferred from the metal to the xenon 6s orbital. Figure 3 shows the density of states on the xenon atom, with the 5p and 6s orbitals showing some broadening and, accordingly, some overlap with the Fermi energy: although this overlap is small, it allows some charge transfer between the metal and the 6s level (around 0.08 electrons) that tends to increase substantially the hybridization and the many-body energy contributions. These effects are clearly seen in Fig. 2b, where the hybridization and the many-body terms show important contributions between distances of 4 Å and 5.5 Å.

Our results show that the short-range interaction is more similar to a typical chemisorption case than to physisorption. In physisorption, the short-range interaction shows a repulsive behaviour that is compensated, around the physisorption energy minimum, by the attractive van der Waals potential. In chemisorption, some bonds are formed between the adsorbate and the substrate. For xenon, we find a precursor of a bond formed between the 6s orbital and the metal; the interaction between that orbital and aluminum is the responsible of having an atractive short-range xenon-aluminum potential due to the charge transfer to the 6s level. This effect appears for distances between 4 Å and 5.5 Å; for shorter distances the high repulsive energy associated with the high electron density of aluminum, prevents the xenon-atom to penetrate the metal.

3.2. Tunneling currents: topography of xenon adsorbed on Al

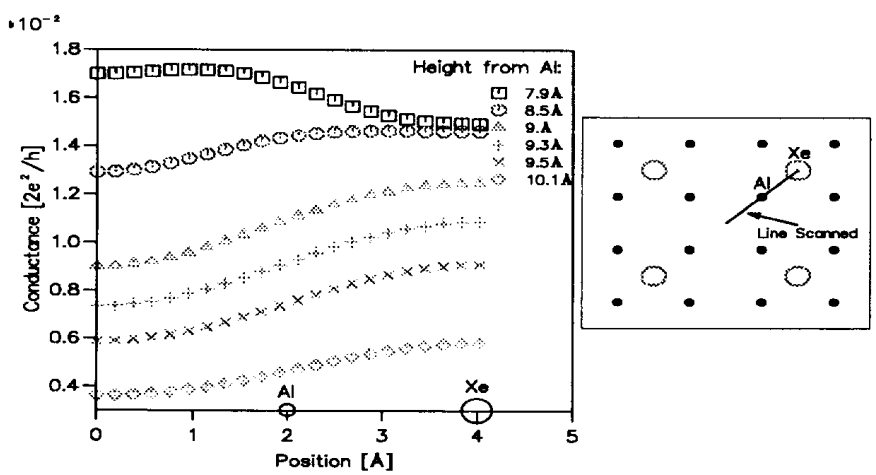

FIG. 4. σ-d curves for different tip-surface distances.

In this section, we analyze the topography of xenon adsorbed on aluminum, by calculating the tunneling currents as described in section 2. The first step is to calculate the electronic

properties of xenon adsorbed on the metal, and to obtain the different quantities, $\rho^0_{AA}(\omega)$ and $G^0_{AA}(\omega)$. Then, (5) and (6) are used to calculate J, the tunneling current: this step can be performed after calculating also independently the tip electronic properties defining $\rho^0_{LL}(\omega)$ and $G^0_{LL}(\omega)$.

The geometry relevant to the tunneling problem has already been introduced in Fig.1: one atom is assumed to be located at the apex of a pyramid having 4 atoms in its base. Each atom of this base is then joined to a Bethe-lattice that simulates the metal bulk density of states. Let us just mention that the electronic properties of this system have been calculated by projecting each Bethe-lattice onto the atom of the pyramid to which it is joined. This allows us to calculate the electron density of states, $\rho^0_{LL}(\omega)$ and the Green-function $G^0_{LL}(\omega)$, by solving the reduced system formed by the atoms of the pyramid located around the tip apex.

In our actual calculations for an aluminum tip, we have taken for the different electron levels parameters given in the standard literature [19], except for the last atom located at the tip apex, whose levels have been described by including the crystal field effects that appear due to the lower symmetry of this atom (details will be published elsewhere).

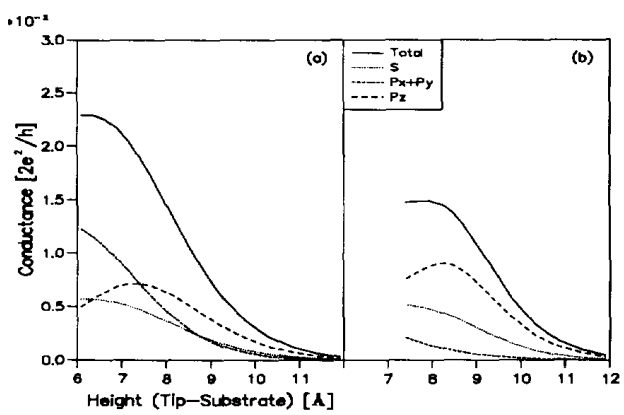

FIG. 5. Current saturation effects. (a) On empty hollow site. (b) On xenon atom.

Figure 4 shows the I-d curve, for constant tip-surface distance and applied bias, when the tip is moved along the direction shown in the inset. Note that our results are obtained for a $p(2 \times 2)$ adsorbed layer, with the xenon occupying the center sites as calculated in the previous section. In this figure, different σ-curves correspond to different tip-surface distances, when the tip is moved along the direction shown in the inset. The current intensity increases when the tip is located atop the xenon atom, except when the xenon-tip distance is too short ($d \leq 8.5$ Å). At these distances, we find an inverted σ-curve associated with the σ-behaviour shown in Fig. 5. Here we show the σ-d curve when the tip is located atop the xenon atom or in an empty hollow site, and moved along the direction perpendicular to the surface. The inverted σ-curves of Fig.4 appear when the conductance for the hollow site gets larger than the one found for the xenon position. In this case, we expect the STM to become unstable because the feedback loop, if operated in the constant current mode, can

find at least two different close heights where the tunneling current takes the same value [21].

Coming back to Fig. 5, it is worth commenting that the σ-d curves are directly related to the surface corrugation that can be measured with the aluminum tip. In particular, we have found that the σ-d curve for $h = 9.25$ Å corresponds to a surface corrugation of around 0.5 Å. Notice that this corrugation is the result of analysing a $p(2 \times 2)$ adsorbed layer, with several xenon atoms affecting the current measured at the hollow site of Fig. 5 (point A in the inset of this figure). We have calculated that for a single xenon atom, the corrugation measured by the aluminum tip can be increased by almost a factor of 3, yielding a value of around 1.5 Å.

Figure 6 shows the complete STM-like image produced scanning over a 9×9 Å^2 area keeping a constant tunneling conductance of $1.8 \times 10^{-2}(e^2/h)$. The (1×1) mesh formed by the aluminum atoms is not visible under these scan conditions and we have put marks to help the reader to visualize the unit cell.

Finally, Fig. 7 shows the σ-d curve for $h = 9.25$ Å, decomposed into the different contributions associated with the different tip-orbitals. From this figure, we see that the s and p_z orbitals contribute to the normal corrugation topography, while the p_x and p_y orbitals tend to yield an inverted topography. This effect explains that the surface topography can depend on the particular electronic configuration found in the tip-apex. Crystal field effects can change the s and p levels and modify substantially the surface topography measured by the particular tip: this shows that the tip geometry can be crucial to the tip resolution (details on these effects will be published elsewhere).

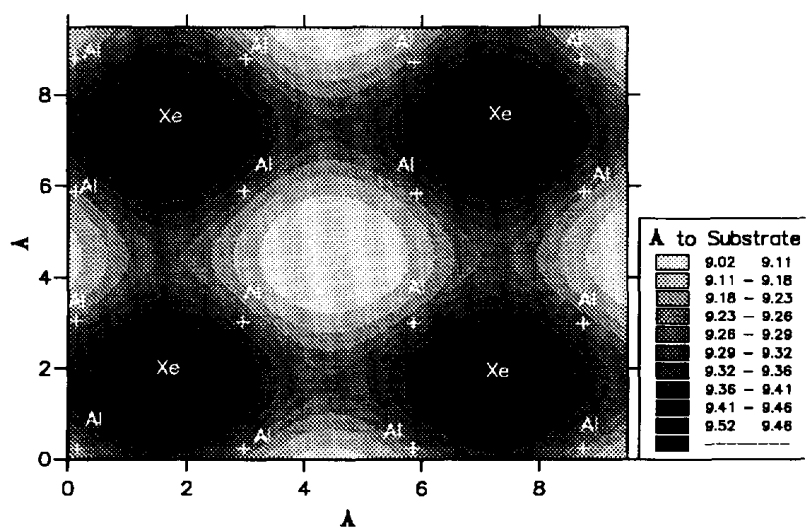

FIG. 6. Atomic STM-like image for Xe/Al(100) at constant tunneling current ($\overline{h} = 9.3$ Å).

4. Conclusions

We present a formalism to obtain a realistic picture for the tunneling current measured with a STM on a surface with or without adsorbed species. Tunneling of electrons between two atoms is related to the bonds between atoms, so we take advantage of this simple physical picture to obtain an accurate approximation to the hopping terms using the Bardeen's tunneling current expression. Therefore, we treat on the same footing two relevant phenomena on surfaces: chemisorption and tunneling. Because the basis of our calculations are the atomic wavefunctions for the different elements in our problem, as obtained from standard calculations in the literature, our approach is a parameter-free one that only depends on the geometrical coordinates of atoms.

In this paper, we present results for Xe on Al(100). The physisorption of xenon on aluminum has been described using the previous approach, and we have shown that the 6*s* level of xenon in its interaction with the metal yields a kind of bonding interaction that makes the short range potential atractive. Having calculated the xenon-metal interaction, we have investigated the STM image of Xe adsorbed on Al(100).

We find the expected corrugation for this system, and we show how saturation effects can affect the results. Our formalism is perfectly suited to study the regime of close contact between tip and adsorbate or surface, as we do not use perturbation theory to obtain the currents and we are fully including multiple scattering effects, believed to be important at such small distances. We observe that the atomic-like nature of the last few atoms on the tip apex are important to explain experimental results, and we include crystal field effects on the energy levels to study the influence of different tip geometries. In this work, we have chosen to keep the structure of the tip as simple as possible (we use aluminum), but work on more complex tips (formed with W or Pt/Ir alloys) is in progress and will be published, shortly.

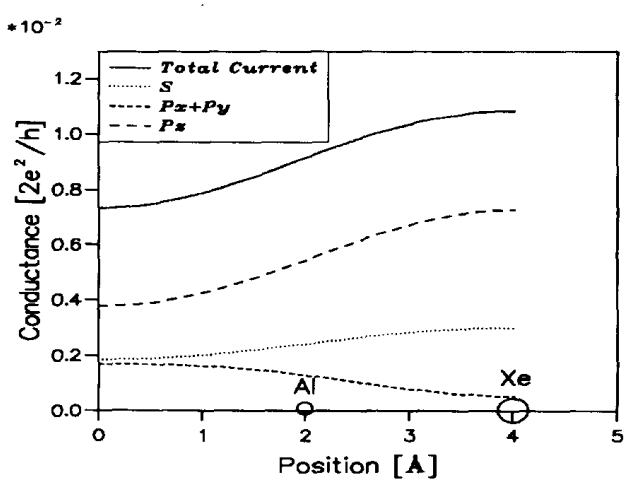

FIG. 7. Different contributions to σ-d curve ($h = 9.25$ Å).

Acknowledgments

The work reported here was partially financed by the Spanish CICYT through contracts Nos. PB92-0168C and PB91-0930. L. Jurczyszyn acknowledges a post-doctoral grant from the Spanish Ministry of Education and Science.

References

1. D.M. Eigler and E.K. Schweizer, Nature **344**, 524 (1990).
2. D.M. Eigler, C.P. Lutz and W.E. Rudge, **352**, 600 (1991).
3. I.W. Lyo and P. Avouris, Science **253**, 173 (1991).
4. H. Uchida, D. Huang, F. Grey and M. Aono, Phys. Rev. Lett. **70**, 2040 (1993).
5. D.M. Eigler, P.S. Weiss, E.K. Schweizer and N.D. Lang, Phys. Rev. Lett. **66**, 1189 (1991).
6. J.R. Cerda, P.L. de Andres, F. Flores and R. Perez, Phys. Rev. B **45**, 8721 (1992).
7. F. Flores, A. Martin-Rodero, E.C. Goldberg and J.C. Duran, Nuovo Cimento D **10**, 303 (1988).
8. E.C. Goldberg, A. Martin-Rodero, R. Monreal, and F. Flores, Phys. Rev. B **39**, 5684 (1988).
9. F.J. Garcia-Vidal, A. Martin-Rodero, F. Flores, J. Ortega and R. Perez, Phys. Rev. B **44**, 11412 (1991).
10. J. Ferrer, A. Martin-Rodero and F. Flores, Phys. Rev. B **38**, 10113 (1988).
11. L.V. Keldysh, Zh. Eksp. Teor. Fiz **47**, 1515 91964) [Sov. Phys. JETP **20**, 1018 (1965)].
12. C. Caroli, R. Combescot, P. Nozieres and D. Saint-James, J. Phys. C **5**, 21 (1972).
13. F.J. Garcia-Vidal, J. Merino, R. Pérez, R. Rincón, J. Ortega, and F. Flores, Phys. Rev. B, in press.
14. W. Kohn and L. Sham, Phys. Rev. A **140**, 1133 (1965).
15 E. Clementi and C. Roetti, At. Data Nucl. Data Tables **14**, 177 (1974).
16. K. T. Tang and J. Peter Toennies, Surf. Sci. **279**, L203 (1992).
17. C. Schwartz and R.J. Le Roy, Surf. Sci. **166**, L141 (1986).
18. A. Chizmeshya and E. Zaremba, Surf. Sci **268**, 432 (1992).
19. D.A. Papaconstantopoulos, *Handbook of the Band Structure of Elemental Solids* (Plenum, N.Y. 1986).
20. A preliminary report of these results was published in R. Perez, F.J. Garcia-Vidal, P.L. de Andres and F. Flores, Surf. Sci. **307/309**, 704 (1993).
21. J.K. Gimzeski and R. Möller, Phys. Rev. B **36**, 1284 (1987).